ISSN 1995-0802, Lobachevskii Journal of Mathematics, 2021, Vol. 42, No. 8, pp. 1753–1767. © Pleiades Publishing, Ltd., 2021.

On the Problem of Resonant Incompressible Flow in Ventilated Double Glazing

T. Akinaga[1*], T. M. Harvey-Ball[2], T. Itano[3***], S. C. Generalis[2****], and E. C. Aifantis[4*****]**

(Submitted by A. M. Elizarov)

[1] *Faculty of Engineering Science, Akita University, 1-1 Tegata-Gakuen Machi, Akita-Shi, Akita 010-8502, Japan*

[2] *Mathematics Department, College of Engineering and Physical Sciences, Aston University, Birmingham B4 7ET, United Kingdom*

[3] *Department of Pure and Applied Physics, Faculty of Engineering Science, Kansai University, Osaka 564-8680, Japan*

[4] *Laboratory of Mechanics and Materials, School of Engineering, Aristotle University of Thessaloniki, Thessaloniki, GR-54124 Greece*

Received April 03, 2021; revised April 19, 2021; accepted April 22, 2021

Abstract—We employ a homotopy method, rather than conventional stability theory, in order to resolve the degeneracy due to resonance, which exists in fluid motion associated with a channel of infinite extent in ventilated double glazing. The introduction of a symmetry breaking perturbation, in the form of a Poiseuille flow component, alters substantially the resonant bifurcation tree of the original flow. Previously unknown resonant higher order nonlinear solutions, i.e. after the removal of the perturbative Poiseuille flow component, are discovered. A possible extension of the methodology to consider non-Newtonian gradient enhanced incompressible viscous fluids is also briefly discussed.

DOI: 10.1134/S1995080221080035

Keywords and phrases: *Incompressible flow, Bifurcation theory, homotopy method, stability, nonlinearity, gradient fluid.*

1. INTRODUCTION AND METHODOLOGY

Studies on natural convection in a fluid layer between vertical parallel plates with infinite extent kept at different temperatures have been investigated continuously since 1950 [1]. The problem arises in the flow of the atmosphere surrounding our planet, in the coolant flow of nuclear reactors, in the air flow within energy efficient buildings and double glazed windows, and in other technological configurations [2].

The classic book of Gershuni [3] provides an account of related research in the field up to the date of its publication. Most notable are Boyarintsev's [1] experiments on laterally heated flows that determined the critical conditions above which the heat conduction state becomes unstable with respect to steady disturbances. Gershuni [3] analyzed the linear stability for this problem with $Pr = 7$ and obtained the critical condition $Gr_c = 13400$: Pr and Gr are the Prandtl and Grashof numbers respectively, while the subscript c denotes the critical value. Later, Korpela and co-workers [4] analyzed the linear stability

*E-mail: akinagat@gipc.akita-u.ac.jp
**E-mail: harveyt1@aston.ac.uk
***E-mail: itano@kansi-u.ac.jp
****E-mail: s.c.generalis@aston.ac.uk
*****E-mail: mom@mom.gen.auth.gr

over a wide range of Pr, specifically, $0 \leq Pr \leq 1000$. They found both steady (for $Pr < Pr_c = 12.7$) and oscillatory (for $Pr > Pr_c = 12.7$) convection. Nagata and Busse [5] analyzed the instability of the secondary nonlinear solutions, bifurcating from the neutral curve, for the isothermal case $Pr = 0$. They analysed the succession of secondary and tertiary steady states with the sequence of bifurcations approach (SBA), and examined their instabilities. They found that in the nonlinear regime, secondary solutions did not exist in a certain wavenumber range outside the neutral curve.

In channels with [6] (and without [7]) system rotation, the Eckhaus stability boundary is found to be a closed loop. Within this boundary, two-dimensional vortices are stable to spanwise and streamwise perturbations. Outside the boundary, vortex pairs may split apart or merge together. For all channels examined in [6], two-dimensional vortices are always unstable when the Reynolds number $Re > 1.7Re_c$, whereas the most unstable spanwise perturbations are subharmonic disturbances: they cause two pairs of vortices with small wavenumbers to split apart by the formation of a new vortex pair; and two pairs of vortices with large wavenumber to merge into a single pair. It was also shown that when Re is not too high ($Re < 4.0Re_c$), the wavenumbers of vortices are selected by the Eckhaus instability and most experimentally observed wavenumbers are close to the ones that are most stable to spanwise perturbations. A similar interaction of two-dimensional vortices, due to the presence of resonance, was the explanation offered in [8], for the lack of ability to numerically identify secondary nonlinear solutions, outside the neutral boundary curve in [5].

In the present paper we show how SBA can serve as an alternative powerful tool for the transition of the undisturbed (basic) flow [9, 10], without the explicit use of traditional stability analysis [11]. This is partly due to the discovery, via the homotopy-SBA combined approach, of coherent solutions [12, 13], that are universal in ubiquitous flows. These coherent structures were discovered without the use of classical stability theory on the (higher order than the laminar) nonlinear solutions, that bifurcate from the basic flow. They have been obtained without the presumption of favourable, or pre-set conditions deduced from empirical arguments, and they exist in a variety of fluid flows as invariant sets, embedded within the turbulent regime. The discovery of these coherent structures indicates that they could be used to probe aperiodic motion in a deterministic way.

Commercial packages offer a range of models for different types of viscous fluid processes and rheology. As the fluid considered in this work (as an example of the general formulation) is assumed to be Newtonian and incompressible, we list below the textbook formulas that govern incompressible Newtonian flow: i.e. the differential statements of mass and momentum balance given by Eqs. (1)

$$\nabla \cdot \mathbf{v} = 0,$$
$$\frac{\rho D\mathbf{v}}{Dt} = -\nabla p - [\nabla \cdot \boldsymbol{\tau}] + \rho \mathbf{g}, \tag{1}$$

where $\mathbf{v}$ is the velocity, $(\nabla\cdot)$ and (∇) are the divergence and gradient operators, ρ is the constant density and D/Dt denotes material time derivative ($D/Dt = \partial/\partial t + \mathbf{v} \cdot \nabla$). Then; $\rho D\mathbf{v}/Dt$ is the mass per unit volume multiplied by acceleration; ∇p is the pressure force per unit volume; $[\nabla \cdot \boldsymbol{\tau}]$ is the viscous force per unit volume; and $\rho\mathbf{g}$ is the gravitational force per unit volume.

The quantity $\boldsymbol{\tau}$ is the stress tensor given by the standard constitutive equation $\boldsymbol{\tau} = -p\mathbf{1} + 2\mu\mathbf{D}$ where p is the pressure, μ is the viscosity constant and $\mathbf{D} = \frac{1}{2}\left[\boldsymbol{\nabla}\mathbf{v} + (\boldsymbol{\nabla}\mathbf{v})^T\right]$ denotes the stretching tensor with $\mathbf{1}$ being the unit tensor, and the superscript T denoting transposition. In the example to be considered later in the paper, non-isothermal conditions will be assumed and, therefore, Eq. (1) will be supplemented by the heat conduction equation where the Laplacian of the temperature field $\nabla^2 T$ will enter. The Laplacian of the stretching tensor $\mathbf{D}$ enters in the constitutive equation for the stress tensor $\boldsymbol{\tau}$ when non-local effects are incorporated as discussed in the Appendix, where an extension of the SBA methodology is proposed to be used for "gradient fluids".

Analytical solutions to the non-linear equations governing fluid motion are limited, and therefore commercial packages use numerical methods based on finite elements in order to seek approximate solutions to flow problems.

This paper is organized as follows: Section 2 describes the mathematical formulation of the problem to be investigated. The basic equations are formulated and discussed and the geometrical configuration is presented. In Section 3 the basic properties of the small gap laterally heated system with an imperfection will be surveyed and the stability characteristics of the nonlinear solutions will be addressed.

In particular, we will outline the stability boundaries of the new states that we have identified, and establish the fully nonlinear solutions up to and including the tertiary level in the sequence of bifurcations approach to turbulence. We conclude with a general discussion of our results and future work in Section 4. Finally, in the Appendix, some remarks on the extension of the present study to include higher-order gradient fluids are given.

2. FORMULATION OF THE PROBLEM

In order to describe in general terms the homotopic SBA that will be followed in this and the next sections, we introduce the generic governing equation of fluid motion:

$$\frac{\partial \mathbf{u}}{\partial t} + \mathbf{L}(\mathbf{R})\mathbf{u} + \mathbf{N}(\mathbf{u}) = \mathbf{0}, \tag{2}$$

where $\mathbf{u}$ describes the deviation from the basic (undisturbed) state of the system, $\mathbf{L}(\mathbf{R})$ is a linear and $\mathbf{N}(\cdot)$ is a nonlinear operator that involve partial derivatives. In Eq. (2) $\mathbf{R}$ represents collectively the parameters of the system, such as the Prandtl or the Reynolds numbers. In our SBA analysis, we first obtain the stability of the basic states via the introduction of infinitesimal disturbances in Eq. (2) by ignoring the nonlinear terms. The nonlinear states grow from the stability boundary of the basic state, that is typically characterised by $f(\mathbf{R}) = 0$, where f is the neutral surface of the basic state. When we repeat the aforementioned procedure of perturbation on the emerged nonlinear states, we find a successive sequence of bifurcations for the higher order states en route to the turbulent state.

From a theoretical viewpoint, let us suppose a numerical channel of infinite extension with gap width $2d$, under periodic boundary conditions with wave numbers α and β in the streamwise and spanwise directions respectively. This channel is the subspace of another numerical channel with the same gap width, but with (subharmonic) wave numbers $\frac{1}{m}\alpha$ and $\frac{1}{n}\beta$, where (m, n) are arbitrary positive integers. An exact equilibrium state realised in the fundamental channel is isomorphic to an exact state in the subharmonic channel.

We consider an incompressible Boussinesq Newtonian fluid, bounded between two vertical parallel planes of infinite extent with different temperatures $T_0 + \Delta T$ and $T_0 - \Delta T$, subject to a pressure gradient deviation from the hydrostatic pressure (Fig. 1). The origin of the Cartesian coordinate system is positioned in the midplane of the fluid layer of width $2d$, And designated by (x, y, z) the streamwise, spanwise and wall normal directions with unit vectors $\hat{\boldsymbol{i}}, \hat{\boldsymbol{j}}, \hat{\boldsymbol{k}}$.

We assume here that the state satisfies periodic boundary conditions with wavenumbers α and β for the x and y directions, respectively. The velocity $\boldsymbol{v}$ and the temperature T are governed by the following equations:

$$\frac{\partial}{\partial t}\mathbf{v} + \mathbf{v}\cdot\boldsymbol{\nabla}\mathbf{v} = -\frac{1}{\rho}\boldsymbol{\nabla}\pi + g\gamma T\hat{\mathbf{i}} + \nu\boldsymbol{\nabla}^2\mathbf{v}, \tag{3}$$

$$\frac{\partial}{\partial t}T + \mathbf{v}\cdot\boldsymbol{\nabla}T = \kappa\boldsymbol{\nabla}^2 T, \tag{4}$$

$$\boldsymbol{\nabla}\cdot\mathbf{v} = 0, \tag{5}$$

where we have incorporated in addition the thermally induced hydrostatic pressure term $g\gamma T_0 x$.

In the above ρ is, as before, the density, κ is the thermal diffusivity, ν (instead of the previously-used μ) is the kinematic viscosity, γ is the coefficient of thermal expansion and g is the magnitude of acceleration due to gravity. For the non-dimensional description of the problem we use d, d^2/ν and $\Delta T/Pr\ Gr$, as the units of length, time and temperature, respectively. The physical properties of the system are characterised by the three non-dimensional parameters $Gr = g\gamma\Delta T d^3/\nu^2$ (the Grashof number that gives the strength of the heating); $Re = U_{\max} d/\nu$ (the Reynolds number) that measures the strength of the applied pressure gradient in the streamwise direction ($U_{\max}$ is the speed of Poiseuille laminar flow at the origin); and $Pr = \nu/\kappa$ (the Prandtl number).

On denoting the non-dimensional form of the velocity, temperature and pressure deviations from the basic state as $\mathbf{u}$, θ and Π, we obtain the non-dimensional form corresponding to Eqs. (3)–(5),

$$\frac{\partial}{\partial t}\mathbf{u} + \mathbf{u}\cdot\boldsymbol{\nabla}\mathbf{u} = -\boldsymbol{\nabla}\Pi + \theta\hat{\mathbf{i}} + \boldsymbol{\nabla}^2\mathbf{u}, \tag{6}$$

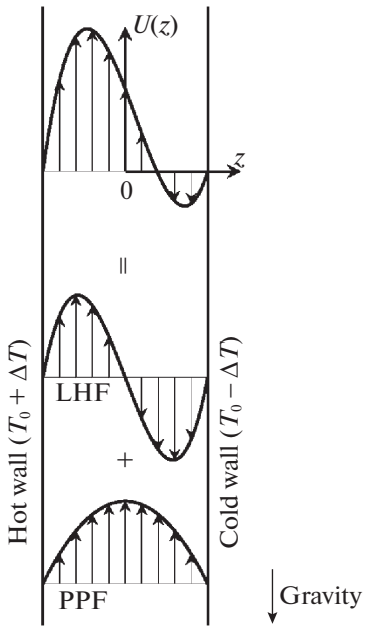

Fig. 1. Geometrical configuration of the problem. The antisymmetric profile for pure Laterally Heated Flow (LHF) deviates from the exactly antisymmetric form (see eq. (9)), under a small perturbation induced by a mean pressure deviation (ie by an added Poiseuille component to the basic flow).

$$Pr\left(\frac{\partial}{\partial t}\theta + \mathbf{u}\cdot\boldsymbol{\nabla}\theta\right) = \boldsymbol{\nabla}^2\theta, \tag{7}$$

$$\boldsymbol{\nabla}\cdot\mathbf{u} = 0. \tag{8}$$

Hereafter, we restrict the scope of our study to the case of $Pr = 0$ ($\kappa \gg \nu$) and two-dimensional flow, (no spanwise dependence of the flow [14]), so that our primary motivation in the present study, the retrieval of resonant modes, via the introduction of symmetry breaking perturbative flows, may be realized simply. At the limit of vanishing Pr (when heat conduction dominates convection) the energy equation (7) decouples from the momentum equation (6) and the temperature variation becomes simply proportional to z, independent of the fluctuations $\mathbf{u}$. Eq. (7) then plays no further role in the analysis. The basic solution (B) of Eqs. (6) and (8), which satisfies the no-slip condition for the velocity ($\mathbf{u} = \mathbf{0}$) on the boundaries at $z = \pm 1$, is given by

$$\mathbf{U}_{\mathrm{B}}(z) = U_0(z)\,\hat{\mathbf{i}},\; U_0(z) = (Gr/6)\left(z^3 - z\right) + Re\left(1 - z^2\right). \tag{9}$$

For the configuration of Fig. 1 Squire's theorem is applicable (see [14]). We further assume that the pressure gradient remains in the mean unchanged by the amplitude of the secondary flow, and we show that there exists degeneracy that is invariably linked with the infinite streamwise length. In order to obtain the (fully nonlinear) equilibrium solution, we introduce the stream function ψ, a function of the (x, z)-variables, with the velocity fluctuations $\widetilde{\mathbf{u}}$ satisfying the relation

$$\widetilde{\mathbf{u}} = \boldsymbol{\nabla}\times\psi\hat{\boldsymbol{j}}. \tag{10}$$

It follows that Eq. (10) ensures that Eq. (8) is satisfied automatically and, thus, Eqs. (6) and (9) describe completely the dynamics of our system. The boundary conditions for ψ are given by

$$\psi = \frac{\partial\psi}{\partial z} = 0 \quad \text{at} \quad z = \pm 1. \tag{11}$$

Two-dimensional steady equilibrium roll solutions are sought numerically, employing the Chebyshev Legendre–Gauss–Lobatto collocation point method combined with the Newton–Raphson iterative

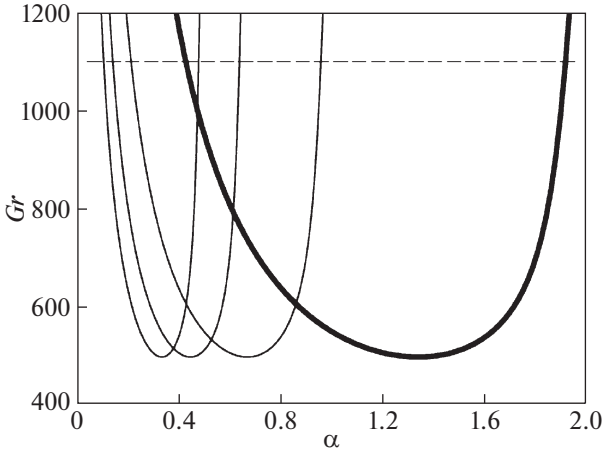

Fig. 2. The neutral curves for the fundamental (thick solid) and subharmonic modes (thin solid) at $Re = 0$, which is described as $Gr = Gr_c(n\alpha, 0)$ $n = 1, 2, 3, 4$. The critical Grashof number is $Gr = 495.6$ at the wavenumber $\alpha = 1.344$. The intersections of the curves, the "bi-critical points", are all candidates of the origins for the nonlinear states generated by a certain nonlinear interaction between the different modes, the pure (nonlinear states from the neutral curve) and the subharmonic neutral curves. This is the so called "resonance".

method, via the following harmonic expansion for ψ:

$$\psi(x,z,t) = \sum_{n=0}^{N} \sum_{\substack{m=-M \\ m\neq 0}}^{M} a_{nm} \left(1-z^2\right)^2 T_n(z) \mathrm{e}^{\mathrm{i}\, m\, \alpha(x-ct)}, \tag{12}$$

where N and M are the truncation levels for the complex coefficients a_{nm}, and $T_n(z)$ is the n-th order Chebyschev polynomial. We have incorporated the phase velocity c in the expansion, so that we can capture additionally the case of moving waves, where a perturbative Poiseuille flow component is allowed to be present (Fig. 1), via the implementation of $Re \neq 0$ in Eq. (9). In this case our frame of reference will be moving with the (exact) phase velocity of the solution and will, therefore, be phase locked with the nonlinear solutions bifurcating from the neutral curve boundaries. In Eq. (12) the factor $(1-z^2)^2$ has been inserted in the expression for ψ, in order to take into account the boundary conditions, expressed by Eq. (11). We also employ additional direct numerical simulations (DNS) for the cases where time dependent solutions that do not lead to shape preserving travelling waves, need to be determined.

For those calculations and in order to determine the bifurcating oscillatory states, perturbations are introduced to the preceding (lower order) states, at the bifurcation point and with parameters (such as wavenumber, Re and Gr) as predicted by our linear stability analysis of the lower order states. The evolution in time of the oscillatory states is analysed through integrations in time of the system of equations for the expansion coefficients in the general representation given by Eq. (12). The truncation level is determined in the same way as in the case of steady state solutions or shape preserving travelling waves. Therefore, M, N are increased up to a level where further increases include small changes (of a few percentage points) to the amplitude of the coefficients of the equations (a_{nm}) in Eq. (12). In this alternative methodology, and in order to determine the stability range of these oscillatory states, we introduce perturbations on the leading coefficients and observe their evolution in time. The (oscillatory) state is considered stable for the range of Reynolds numbers for which a converged solution can be identified. Further details of the numerical method employed here, in order to identify nonlinear solutions, have been presented recently to different types of shear flows [12, 13, 15].

3. RESULTS

3.1. Linear Stability

We define the neutral stability curve, as the curve that provides the critical Gr number as a function of the wavenumber α at a pre-specified value of Reynolds number, $Gr_c(\alpha, Re)$.

Table 1. Wavenumber and Grashof number values of the bi-critical points, $(\alpha_{c,n}, Gr_{c,n})$, for $Re = 0$. These bi-critical points are determined as the solution of $Gr_c(\alpha, 0) = Gr_c(n\alpha, 0)$. At the bi-critical point, the nonlinear branch may be generated from a certain nonlinear interaction between the fundamental and subharmonic modes. For example, the branch T, shown in Fig. 4, originates from F_{3-2} that bifurcates from the first bi-critical point, $(\alpha_{c,2}, Gr_{c,2})$, listed in this table (see also Fig. 2)

n	$\alpha_{c,n}$	$Gr_{c,n}$
2	0.8631	604.3
3	0.6166	791.9
4	0.4761	999.9
5	0.3879	1212.7
6	0.3277	1426.1
7	0.2839	1639.1
8	0.2506	1851.9

Table 2. Comparison of nonlinear results with [16] for the energy E_1 of Eq. (13) of the pure mode for various (Gr, α) values. In the present work the truncation level $(L, M) = (21, 18)$ has been used for all nonlinear calculations. In [16] for the nonlinear calculations $L = 40$ was employed with the value of M as indicated

Gr	α	[16]	This work ($M = 18$)
500	1.25	2.41706×10^{-4} (4)	2.41746×10^{-4}
500	1.30	2.53302×10^{-3} (4)	2.53306×10^{-3}
600	0.90	9.25916×10^{-4} (6)	9.25916×10^{-4}
600	1.30	6.14480×10^{-2} (6)	6.18481×10^{-2}
2000	2.00	1.88510×10^{-1} (12)	1.88509×10^{-1}
5000	1.30	3.70190×10^{-2} (16)	3.70657×10^{-2}

In Fig. 2, the neutral curve $Gr = Gr_c(\alpha, Re = 0)$, is given as a thick solid curve on the α-Gr plane. The thin solid curves, on the left hand side of the α-Gr plane, are also neutral curves, but they depict the $Gr_c(n\alpha, 0)$ relationship in the case where α has been scaled by a factor $1/n, n = 2, 3, 4$. These curves are described by the functional relationship $Gr = Gr_c(n\alpha)$ and we term them subharmonic neutral stability curves.

At a given $Gr > Gr_c(n\alpha, 0)$, an infinitesimal disturbance added onto the basic flow may grow exponentially. The eigenfunction generated from $Gr_c(\alpha, 0)$ is referred to as the fundamental mode, while the eigenfunctions generated from the 'duplicated' modes, i.e. those from $Gr_c(n\alpha, 0)$ $(n = 2, 3, 4)$, are referred to as *subharmonic modes*.

3.2. Resonance in the Infinite Extent Case

It is possible that any combination that consists of a number of eigenmodes associated with the neutral curves, can develop into some resonant nonlinear state in the system with infinite extent. The case of the conventional Rayleigh–Benard convection is an example, where, square or hexagonal cells are generated by the combination of two or three self-resonating eigenmodes.

In Table 1, we list the specific parameter values (α, Gr), for the bi-critical points, at which the neutral stability curve intersects the subharmonic stability curves, $Gr_c(\alpha) = Gr_c(n\alpha)$ $(n > 1)$. At these parameter values the fundamental mode may interact the subharmonic modes, so that a nonlinear state can be established.

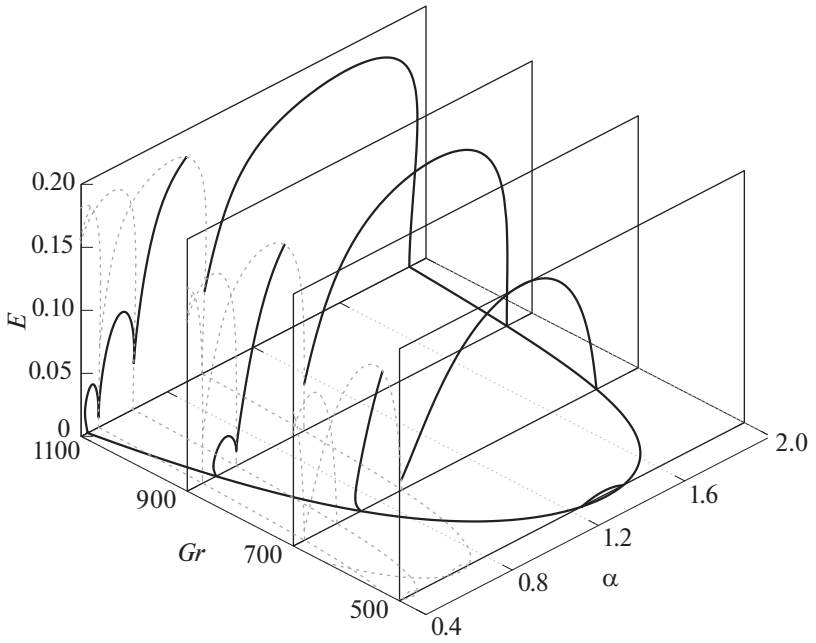

Fig. 3. Global bifurcation picture for $Re = 0$. This figure also extends Fig.3, since the right most part of the nonlinear bifurcation curves are shown. Here the states with $Re = 0$ are shown. At the right part of the neutral curve, and for $Gr \gtrsim 900$, bifurcations are subcritical, while from the left hand side (of the neutral curve), bifurcations are subcritical for $Gr \gtrsim 700$. Dashed curves on the left hand side of the neutral curve represent resonant nonlinear bifurcation curves.

3.3. Previous Work

Previous studies, [8, 16, 17] on the subject have left ambiguous points in their attempts to clarify the nature of the interaction that the fundamental and subharmonic modes play.

For the case of $Re = 0$ in [5], equilibrium states were calculated, which should be expected to bifurcate from $Gr_c(\alpha, 0)$. The finite-amplitude equilibrium states were obtained for a much narrower range than expected (see Fig. 3 of [5]). We will now explain this discrepancy.

Suppose that the laminar state loses its stability at a given Gr against a perturbation with the wave number α satisfying $\alpha_- < \alpha < \alpha_+$, where $\alpha_\pm$ are the solutions of $Gr = Gr_c(\alpha, 0)$.

In [17] it was claimed that the equilibrium state can exist only in the range of wave number $\alpha_+/2 < \alpha < \alpha_+$ and, thus, these authors could partly account for the discrepancy encountered in [5] as mentioned above. By employing weakly nonlinear analysis, they showed the possibility that an interaction of the fundamental with the subharmonic mode may constitute a nonlinear equilibrium state with subharmonic wave number, which was not obtained in [5]. Their study, though, left the region $\alpha_- < \alpha < \alpha_+/2$ unaccounted for.

The occurrence of resonance in Rayleigh–Benard convection was reported in [8], where the discrepancy in the bifurcation diagram of [18] was accounted for, by attributing one of the 'hidden' states as the state generated by the mutual interaction between the fundamental and subharmonic modes n $(= 2, 3, 4, \cdots)$, coining this $1 : n$ resonance.

In Table 2 we show a comparison between our nonlinear results and those of [16] for the value of E_1 defined in Eq. (13).

3.4. Introduction of the Symmetry Breaking Perturbation $Re \neq 0$

In the following, we will show a previously unknown nonlinear branch, which connects to the nonlinear branches emerging from the neutral stability curve $Gr_c(\alpha, 0)$ and its duplications (resonant curves) $Gr_c(n\alpha, 0)$ $(n = 2, 3, 4)$.

We discover the unknown nonlinear branch, by introducing a perturbation (in the form of a small plane Poiseuille flow component) to the system with $Re = 1$. Although the introduced value, $Re = 1$,

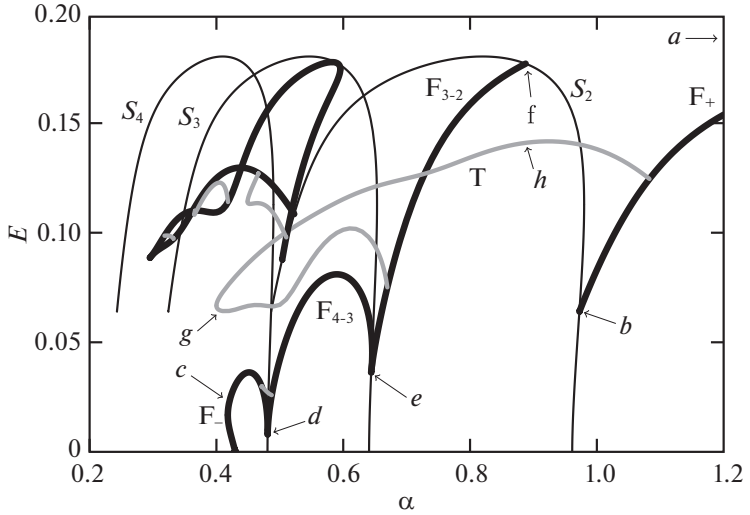

Fig. 4. Nonlinear branches at $(Gr, Re) = (1100, 0)$. The thick curves, marked by $F_{\pm}$, are the secondary branches bifurcated directly from the basic state on the neutral curve, $Gr = Gr_c(\alpha, 0)$. The curve, marked F_-, connects to the (E)-curves of F_{4-3} and F_{3-2} sequentially, that in turn connect with the thin curves, marked with S_n, which refer to the n-th subharmonic duplications of the F_+. The gray curve, named by the symbol T, and the other gray curves correspond to traveling wave solutions. The lower case lettering $(a - h)$ corresponds to the location in the graph, where the corresponding flow pattern(s), illustrated in Fig. 5, are obtained.

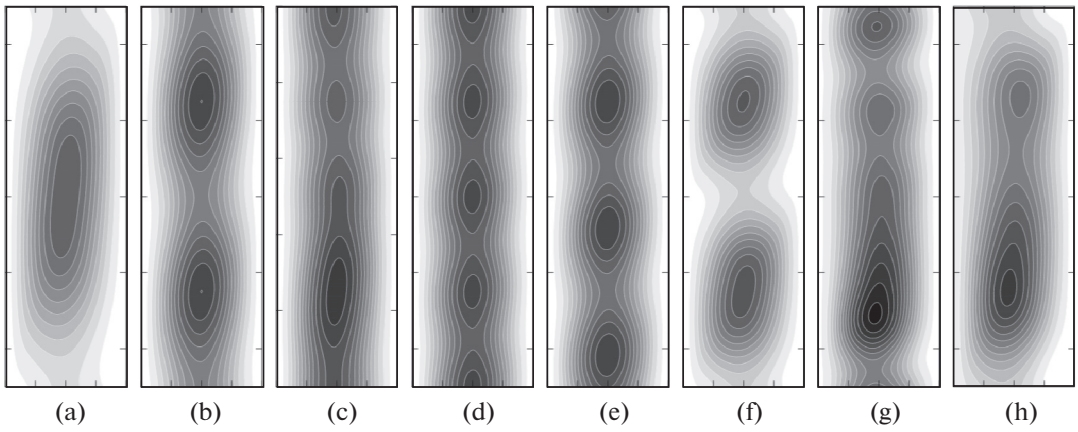

Fig. 5. Contour plots for stream function for $Gr = 1100$, $Re = 0$. The contour levels are indicated in light grey scale for small and in dark grey scale for large values and for: (a) $\alpha = 1.60$ on F_+, (b) $\alpha = 0.98$ on F_+, (c) $\alpha = 0.42$ on F_-, (d) $\alpha = 0.48$ on F_-, (e) $\alpha = 0.64$ on F_{4-3}, (f) $\alpha = 0.88$ on F_{3-2}, (g) $\alpha = 0.42$ on T, (h) $\alpha = 0.88$ on T. In each plot the state between the boundaries is depicted for one wavelength in the ordinate. The location (a)–(h) of the corresponding flow pattern in the (α, Gr) plane is indicated in Fig. 4. See also Fig. 7.

seems to be subtle and rather unwarranted, the resulting bifurcation diagram is substantially richer than that obtained by means of the classical step-by-step procedure of SBA. The subtlety of our mechanism, imposed by introducing a symmetry breaking perturbation, is displayed by the fact that the uncovered nonlinear state in the diagram at $Re = 1$ survives even when $Re = 0$, i.e., when the induced perturbation is removed, as we explain below.

3.5. The Resonant Region

By introducing a perturbation that breaks the symmetry of the basic state, see Eq. (9), we can obtain the spectrum of all possible resonant nonlinear states at $Gr = 1100$ and $Re = 0$ (see Fig. 4~~(a)~~ and Fig. 7). In order to do this, we follow [19] and we characterise states in terms of the kinetic energy (where

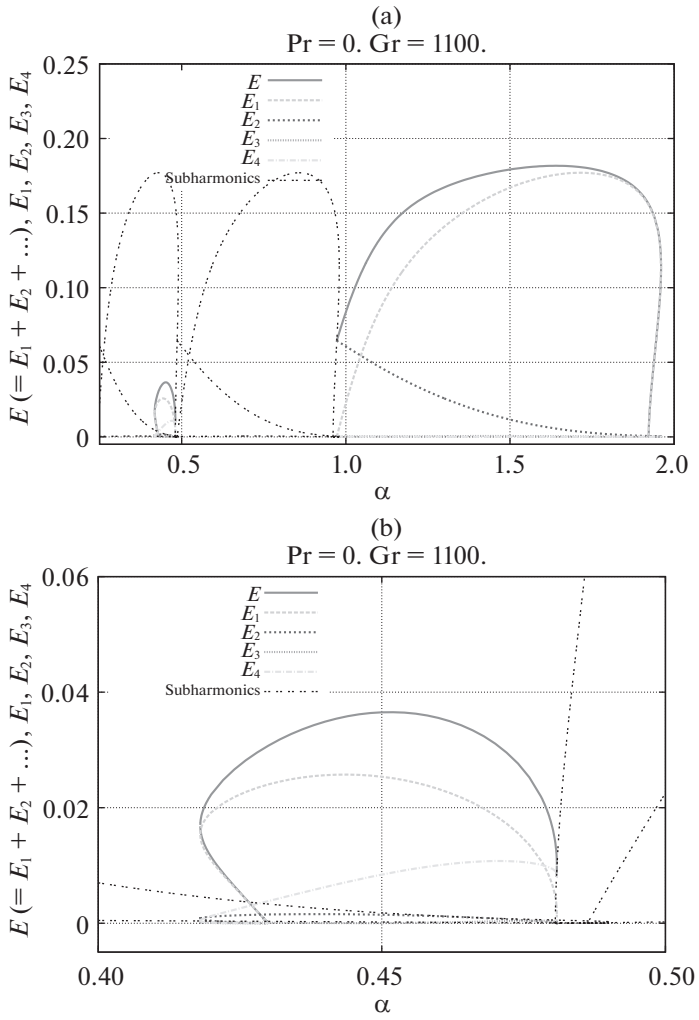

Fig. 6. 2 : 1 and 4 : 1 resonant states for $\alpha = \alpha_+ \approx 1.0$(a) and $\alpha = \alpha_- \approx 0.4$((b) – corresponding enlarged region in (a)), respectively. The states at the bifurcation points have only sub-energy E_j ($j = 1, 2, 3, 4$) defined by Eq. (13).

E represents the total and E_m the individual modal component of kinetic energy) of the fluctuation normalised with respect to the basic flow:

$$E = \sum_{m=1}^{m=\infty} E_m, \quad E_m = \frac{15}{8} \int_{-1}^{+1} \int_{0}^{2\pi/\alpha} |\boldsymbol{\nabla} \psi_m|^2 dx dz, \tag{13}$$

$$\psi_m = \sum_{n=0}^{N} \psi_{nm} + \overline{\psi_{nm}}, \tag{14}$$

where $\overline{\psi_{nm}}$ is the complex conjugate of ψ_{nm}.

In Fig. 4, the secondary branches bifurcated from the neutral curve $Gr_c(\alpha, 0)$ at $\alpha = \alpha_\pm$ for $Gr = 1100$ are depicted as thick curves with the symbol $\mathrm{F}_\pm$; i.e. $\mathrm{F}_\pm$ stands for the secondary state that bifurcates from the *fundamental* neutral curve with wavenumber value $\alpha_\pm$.

The three thin curves, S_n, are duplications (or subharmonics) with scale factors n ($= 2, 3, 4$) of F_+. In our study, S_n stands for the secondary state which bifurcates from the *subharmonic* neutral curve at $\alpha_\pm/n$, while, T stands for a tertiary (travelling wave) state that has bifurcated from the secondary states. In the following, the association between S_n, $\mathrm{F}_\pm$, T and their corresponding properties, based on Figs. 4 and 5, are discussed.

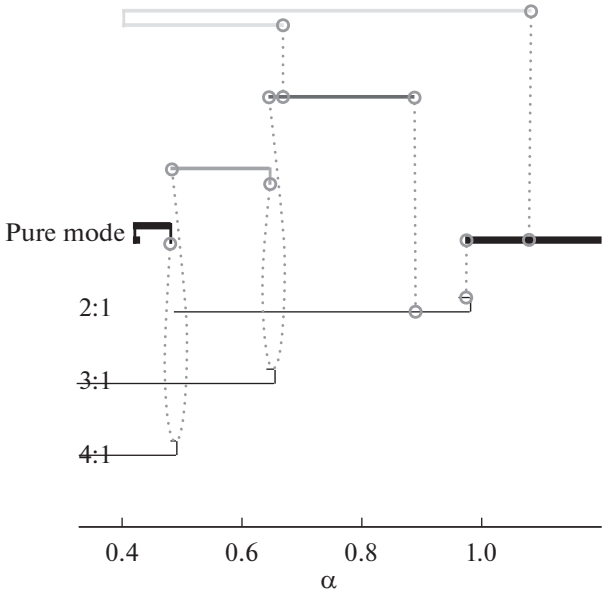

Fig. 7. Connections of resonant and pure mode nonlinear branches. This figure should be viewed in conjunction with Fig. 4. Here $Gr = 1100$, $Re = 0$. In this figure and from left to right the thick solid lines depict the wavenumber range of the secondary pure state F_{-}, the two resonant secondary states F_{4-3}, F_{3-2} and the pure secondary state F_{+}. The tertiary state T is the uppermost line depicted.

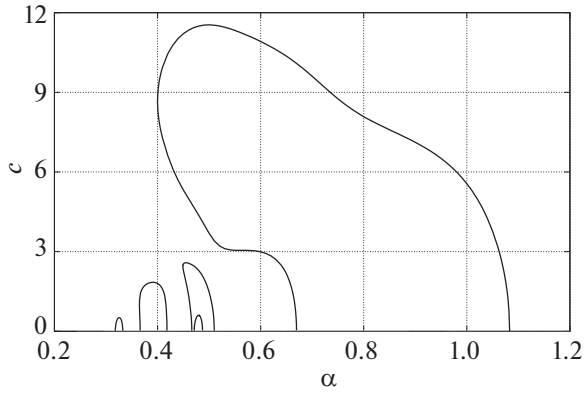

Fig. 8. Phase velocities c for $Gr = 1100$ and $Re = 0$ of the tertiary states (including T) indicated by the thick light grey curves of Fig. 4.

Branch F_{+} which bifurcated from the neutral curve at $\alpha_{+}(= 1.922)$ (only the part $E \leq 0.2$ of F_{+} is shown in Fig. 4) terminates at the intersection on S_2, which is characterised by $\alpha = 0.973$. Along the F_{+} as the wavenumber α decreases, the flow pattern changes from single vortex state (Fig. 5(a)) to two vortex state (Fig. 5(b)). On the other hand, F_{-} that bifurcated from the left hand side of the neutral curve at α_{-} $(= 0.430)$ terminates at $\alpha = 0.481$ on S_4. Along the F_{-} as α increases, the flow pattern changes from single vortex state (Fig. 5(c)) to four vortex state (Fig. 5(d)). The branch F_{-} joins with the branch F_{4-3} at $\alpha = 0.481$ on S_4, and F_{4-3} connects to a branch F_{3-2} at $\alpha = 0.644$ on S_3. Here F_{m-n} $(m, n$ integers) refers to the nonlinear state that bifurcated from the neutral curve and that exists in the m, n resonant region. At the intersection on S_n the n vortex state (Fig. 5(d)–(f)) is always observed.

Finally, F_{3-2} terminates at the node (intersection) at S_2. There is only the branch S_2 between $\alpha = 0.888$ and 0.976. We also note here that the first Fourier mode is absent for the branch S_2. We have thus accounted for the gap that was the mysterious region (where no state could be found) in the previous study [5]. We have therefore, with this exposition, explored the entire resonant region up to and including $4:1$ resonance. These nonlinear states have been obtained for parameter values that are far away from the vicinity of bifurcation points, where our nonlinear analysis is still valid (see [8, 16, 17]).

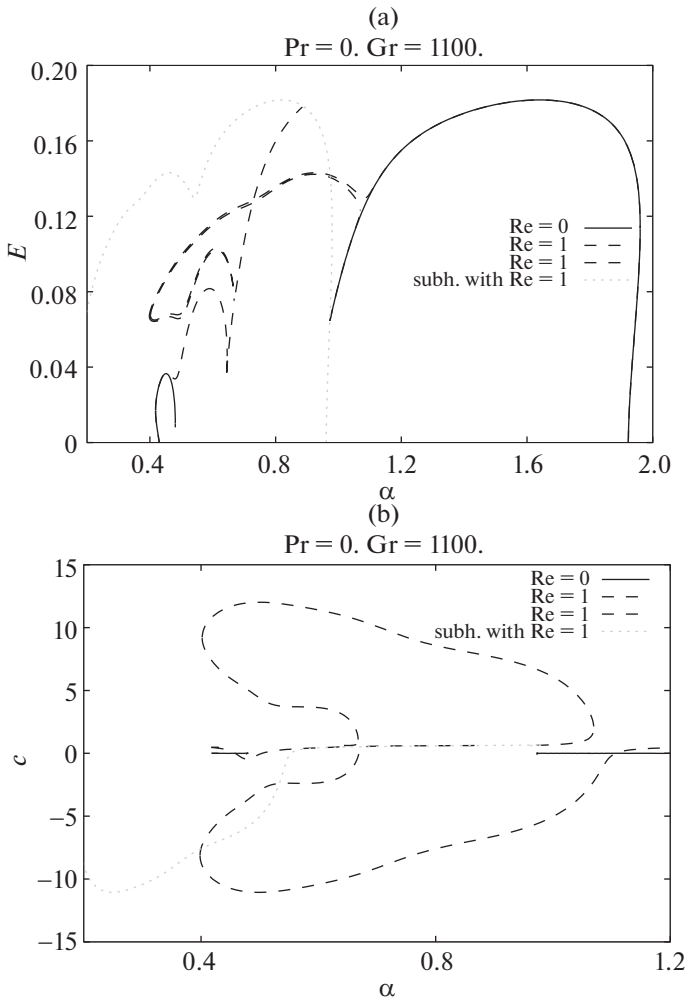

Fig. 9. The extended bifurcation diagrams of the nonlinear states, including F_+, which bifurcates subcriticaly for (a) Energy (E) and (b) phase velocities (c). Here $Pr = 0$ and $Gr = 1100$. This figure extends Fig. 4 by showing the right-most part of the nonlinear curves. The phase velocities for the states with $Re = 0$ and $Re = 1$ are shown here for the case of $Gr = 1100$. For $Re = 0$ the nonlinear states are monotonic ($c = 0$), while for $Re \neq 0$ we have a pair of opposite travelling waves.

3.6. Resonance $n : m$

In order to see in detail the bifurcations at $(Gr, Re) = (1100, 0)$ depicted in Fig. 4, the mean energy E of the subharmonics of the pure modes and the energies for each Fourier mode are superposed onto Fig. 6. The branch from the right side can be extended until the pure mode and the 1:2 subharmonic mode meet. Initially the growth of E_1 is dominant, while E_2 grows slowly. Energy components, except E_2, tend to zero at the left hand side. This suggests that the solution here (at the left hand end) is the same as the solution where the E curve intersects the E_2 curve.

Similarly, in the enlargement (Fig. 6(b)) around the left bifurcation point in Fig. 6(a), the solution bifurcated from the left hand side ends where the subharmonic of the pure mode with quarter wave number exists. The energy component of the 4th mode of the Fourier E_4 is almost the same as E. We conclude that $4 : 1$ resonance inhibits the extension of the solution and that the left branch is inside the resonant region. As a result of this mechanism, there exists a regime between these ends (bifurcation points), where no two-dimensional solutions (from the neutral curve) exist.

3.7. The Discovery of the Branch T

Branch T in Fig. 4 corresponds to a nonlinear state uncovered within our procedure and would have remained undetected if the symmetry breaking perturbation had not been introduced. We should

emphasise that even at $Re = 0$, the branch T possesses a non-zero phase velocity c which originates from the system that was perturbed with $Re = 1$. If we select the opposite sign ($Re = -1$), the same kind of solution drifting in the opposite direction is obtained. Therefore, two drifting solutions have been identified: one via homotopy and a second followed by its reversal.

Extending over the previously unexplained gap, the branch T forms a bridge between the branches F_+ and S_{3-2}. The contour plot of T is given in Fig. 5(g) and (h), which are somewhat reminiscent of the vortices in Fig. 5(c) and (f). The origins of T were previously unexplained, although some indications of its existence had been made. For example, one may refer to the existence of the mixed mode suggested by Fujimura and Mizushima [17] as mentioned earlier. Even though they obtained evidence of its existence only for a few sets of parameters by using a weakly nonlinear analysis valid only in the vicinity of the neutral curves. Our results are fully nonlinear and our calculations are therefore valid away from the vicinity of the neutral curves.

3.8. Remainder of Nonlinear Branches

Our numerical simulations have revealed several additional nonlinear branches, which are shown on the left hand side of Fig. 4.

Besides the additional branches shown in the region $0.29 \leq \alpha \leq 0.59$, we have also depicted a sample of tertiary states to keep the figure uncluttered. The branches S_n serve as the platform for bifurcation of three higher order distinct branches in the regions, $0.467 \leq \alpha \leq 0.510$, $0.316 \leq \alpha \leq 0.418$, and $0.318 \leq \alpha \leq 0.333$. Moreover, another tertiary state was found in a tiny region $0.4712 \lesssim \alpha \lesssim 0.4873$.

All the branches indicated by thick curves, including T, possess non-zero phase velocities, even at $Re = 0$, i.e. when the Poiseuille component is removed. The phase velocities as functions of the wavenumber α, $c = c(\alpha)$, are given in Fig. 8.

4. CONCLUDING REMARKS

We summarise our results and offer some further details of our work as follows:

4.1. Subcriticality

It is of interest first to note a subtle change in the bifurcation diagram on the $\alpha - Gr$ plane occurring at the wavenumber α_+ between $Gr = 900$ and 1100. The bifurcation of the nonlinear branch, F_+ from the basic state is supercritical at $Gr = 900$. However, for $900 < Gr < 1100$, the bifurcation of the nonlinear state F_+ becomes subcritical.

This is better shown in Fig. 3, where bifurcations are shown for $Gr \geq Gr_c$, along with the subharmonic nonlinear states bifurcated from the resonant neutral curves. Around $Gr \gtrsim 600$, the nonlinear states (thick curves) become disconnected due to $1:2$ resonance. At higher Gr we have additional gaps due to $1:3$ ($Gr \gtrsim 800$), $1:4$ ($Gr \gtrsim 1000$), $2:3$ ($Gr \gtrsim 850$), $3:4$ ($Gr \gtrsim 1100$) resonances. Similar behaviour, but in a different context, has been noticed in [13].

In Fig. 9(a) the states with the addition of a small Poiseuille component to the basic flow ($Re = 1$) are also shown. The removal of the Poiseuille component exposes these, otherwise hidden, states that remain present in the case of pure laterally heated flow ($Re = 0$).

4.2. Topological Change of the Bifurcation Diagram with Increase of Gr

We comment next on the topological change of the bifurcation diagram with decreasing values of Gr.

Although it is not illustrated in Fig. 3, for $Gr = 500$ around the critical Grashof number, the bifurcation of the nonlinear branch is supercritical at $\alpha_\pm$ and has the maximum value of E at $\alpha \approx (\alpha_+ + \alpha_-)/2$, as it is a convex single curve. The corresponding nonlinear branch does not exhibit phase velocity (stationary nonlinear solution).

This is not the case for higher values of Gr, where the single curve of the nonlinear state fragment above the bi-critical point, that is ($Gr > Gr_{c,2}$) due to the existence of 'resonance', as shown clearly in Fig. 4. At the bi-critical point, where the break-up occurs, the two split branches are connected with the hidden resonant neutral curve T.

4.3. Topological Change of the Bifurcation Diagram from $Re = 1$ to $Re = 0$ (Poiseuille Flow to Laterally Heated Flow)

Initially, the pure mode nonlinear solution which bifurcates from the neutral curve at $\alpha = 1.9223$ (see Fig. 9; see also Fig. 3 for comparison purposes) has a phase velocity $c = 0.61447$, due to the presence of Re, following the path of the pure laterally heated flow. But, at $\alpha = 1.06961$, the pure mode (that bifurcates from the left hand side of the neutral curve) folds and continues within the resonant region, where it connects with the subharmonic $1:2$ resonant mode at $\alpha = 0.8850$. Similarly, the solution that bifurcates from the left hand side of the neutral curve at $\alpha = 0.4299$ (with phase velocity $c = 0.48633$) also connects with the $1:2$ resonant mode branch at $\alpha \approx 0.97251$.

Therefore the entire branch of the secondary state extends naturally over to the resonant region via two drifting waves with opposite phase velocities. Both drifting waves connect with the 1:2 subharmonic (resonant) nonlinear solution. Finally, as shown in Fig. 9(b), the phase velocities of these two secondary branches (including their loops) bridge the disconnected parts of the E_1 curve and the $1:2$ subharmonic (resonant) region for ($Gr = 1100$, $Re = 0$) over a range of the wavenumber α values. This is shown explicitly in Fig. 4, where the tertiary state T connects F_+ and F_{3-2}.

4.4. Advantage of the Procedure

The measure of the influence of the Poiseuille flow component Re on the bifurcation spectrum of the laterally heated flow without the Poiseuille flow component is shown in Fig. 4, where we removed the imposed constant pressure gradient. The important aspect here is to note that the connecting secondary nonlinear states (extensions of the E_1 curve for the case $Re = 1$ and embedded in the resonant region) remain, even if we remove the added value of Re; thus, returning to the case when $Re = 0$ (i.e. pure laterally heated flow).

In other words, while for $Re = 1$ there are topologically two $E-$curves that naturally connect the pure mode (bifurcating from the right and left hand side of the neutral curve) with the disconnected branches and the resonant bifurcation branches (via the introduction of the oppositely moving drifting waves), the topology of the bifurcation tree changes substantially for $Re = 0$. The difference (when the constant pressure gradient has been removed, $Re = 0$), is that the connecting branches break-up now and the discontinuity points become bifurcation points of higher order, i.e. tertiary states.

For the comparison of the two cases ($Re = 0, 1$), see Fig. 9(a). The presented methodology in this manuscript points to the fact that it is possible to control transition of shear flows for creating more stable and efficient double glazed windows, through the newly discovered resonant states. This will enable producers of glazing products to reduce significantly the heat lost (winter) or gained (summer) through windows, with obvious advantages for society, economy and the environment.

Acknowledgments. TA acknowledges the financial support from the Horizon 2020 Marie Sklodowska Curie Programme of the European Union. SG acknowledges financial support from ORDIST of Kansai University. TI acknowledges an International Collaboration fund from Aston University. THB acknowledges a research studentship from EPSRC DtP 2020. This work was also funded by the RISE-2018 — 824022-ATM2BT of the European H2020-MSCA programme.

Appendix A

GRADIENT FLUIDS

At small microscopic and molecular scales, non-local effects are important and a robust way to account for them is to use higher-order spatial gradients to enter in the consitutive equation for the Newtonian stress $\boldsymbol{\tau}$. One effective way to do this is to employ the internal length gradient (ILG) framework recently reviewed by the last author [21, 22]. In the present case of incompressible Newtonian fluids, this amounts to replacing the standard expression for $\boldsymbol{\tau}$ by the weakly non-local gradient constant given by the equation below:

$$\boldsymbol{\tau} = -p\mathbf{1} + 2\mu(1 - l_{\mathbf{D}}^2\nabla^2)\mathbf{D}, \tag{A1}$$

where $l_{\mathbf{D}}$ is an internal length parameter accounting for weakly non-local gradient effects. The introduction of the Laplacian is not arbitrary, but it arises from a Taylor series expansion of a non-local

integral expression for the average (macroscopic) stress which, by retaining terms up to the second order in the Taylor series expansion, is replaced by the local (microscropic) stress and its Laplacian multiplied by the internal length parameter $l_{\mathbf{D}}$ as shown in Eq. (A2).

The determination of the new phenomenological parameter $l_{\mathbf{D}}$ is left to experiments and simulation, and the same holds for the new type of boundary conditions that the Laplacian term requires. Among the implications of Eq. (A2) are the elimination of singularities and the revision of boundary layer estimates, as well as the interpretation of size effects that classical theory is not able to capture. Equally important is the new possibility that is offered for relocating the Eckhaus stability boundary and to obtain new results by applying the homotopy-SBA method. All this will be a subject of a future series of articles.

For the purposes of the present article, however, we list below the governing equation of motion implied by Eq. (A1), i.e. the modified, gradient enhanced Navier–Stokes (NS) equations of incompressible flow:

$$\rho\frac{D\mathbf{v}}{Dt} = -\nabla p + \mu(\Delta\mathbf{v} - l_D^2\Delta^2\mathbf{v}), \tag{A2}$$

where $\Delta = \nabla^2$ and $\Delta^2 = \nabla^4$ denote the Laplacian and biharmonic operators respectively. It is noted that Eq. (A2) is identical to the equation used to model plane Poiseuille liquid flow at small-length scales as discussed in [20, 21]. A slightly generalized model was also used by the authors to consider turbulence. The governing differential equations for this model reads

$$\rho\frac{D\mathbf{v}}{Dt} = -\nabla p + \mu(1 - \alpha^2\Delta\mathbf{v})\Delta\mathbf{v} + 2\rho\alpha^2\mathrm{div}\overset{\nabla}{\mathbf{D}}, \tag{A3}$$

where the α parameter denotes a statistical correlation length and $\overset{\nabla}{\mathbf{D}} = \dot{\mathbf{D}} + \mathbf{DW} - \mathbf{WD}$ denotes the usual Jaumann rate ($\mathbf{W} = \frac{1}{2}\left[\nabla\mathbf{u} - (\nabla\mathbf{u})^T\right]$).

Steady-state solutions of Eq. (A2) may be determined by employing the operator split method (or the use of Ru–Aifantis theorem [20, 21]) utilized to eliminate singularities from dislocation lines and crack tips in the theory of gradient elasticity. This same procedure leads to the cancelation of singularities in typical fluid flow calculations involving immersed objects. It turns out, for example, that the resulting gradient Oseen tensor $\mathcal{O}_{ij}^G$, which generalizes its classical counterpart $\mathcal{O}_{ij}$

$$\mathcal{O}_{ij} = \frac{1}{8\pi\mu r}\left(\delta_{ij} + \frac{r_i r_j}{r^2}\right), \tag{A4}$$

where r_i denotes the position vector and r its magnitude, reads

$$\mathcal{O}_{ij}^G = \frac{1}{8\pi\mu r}\left\{\left[1 - 2e^{-r/l} - \frac{2l}{r}e^{-r/l} + \frac{2l^2}{r^2}(1 - e^{-r/l})\right]\delta_{ij} + \left[1 + 2e^{-r/l} + \frac{6l}{r}e^{-rl} - \frac{6l^2}{r^2}(1 - e^{-r/l})\right]\frac{r_i r_j}{r^2}\right\}. \tag{A5}$$

More details on gradient fluids can be found in [21]. In a forthcoming publication, the methodology outlined in Section 2 will be utilised to analyse Eq. (A2) in place of Eq. (1) listed in Section 1.

It is expected that new solutions and stability branches will be found. This expectation is partly suggested by the new shear band solutions obtained within the ILG framework for gradient plasticity by employing the homotopy method [22].

REFERENCES

1. D. I. Boyarintsev, "On the stability of three-dimensional disturbances of viscous flow between parallel walls," Zh. Tekh. Fiz. **20**, 1084 (1950).
2. T. Akinaga, T. Itano, and S. C. Generalis, "Convection induced by instabilities in the presence of a transverse seepage," Chaos Solitons Fractals **91**, 533–543 (2016).
3. G. Z. Gershuni and E. M. Zhukhovitskii, *Convective Stability of Incompressible Fluids* (Keterpress Enterprises, Jerusalem, 1976).
4. S. A. Korpela, D. Gőzüm, and C. B. Baxi, "On the stability of the conduction regime of natural convection in a vertical slot," Int. J. Heat Mass Transfer **16**, 1683–1690 (1973).

5. M. Nagata and F. Busse, "Three-dimensional tertiary motions in a plane shear layer," J. Fluid Mech. **135**, 1–26 (1983).
6. Y. Guo and W. H. Finlay, "Splitting, merging and wavelength selection of vortices in curved and/or rotating channel flow due to Eckhaus instability," J. Fluid Mech. **228**, 661–691 (1991).
7. R. Clever and F. Busse, "Transition to time-dependent convection," J. Fluid Mech. **65**, 625–645 (1973).
8. J. Mizushima and K. Fujimura, "Higher harmonic resonance of two-dimensional disturbances in Rayleigh-Benard convection," J. Fluid Mech. **234**, 651–667 (1992).
9. F. Busse, "The sequence-of-bifurcations approach towards understanding turbulent fluid flow," Surv. Geophys. **24**, 269–288 (2003).
10. G. Kawahara, M. Uhlmann, and L. van Veen, "The significance of simple invariant solutions in turbulent flows," Ann. Rev. Fluid Mech. **44**, 203–225 (2012).
11. T. Akinaga, S. C. Generalis, and F. Busse, "Tertiary and quaternary states in the Taylor-Couette system," Chaos Solitons Fractals **109**, 107–117 (2018).
12. T. Itano and S. Generalis, "Hairpin vortex solution in planar couette flow: A tapestry of knotted vortices," Phys. Rev. Lett. **102**, 114501 (2009).
13. S. Generalis and T. Itano, "Characterization of the Hairpin vortex solution in plane Couette flow," Phys. Rev. E **82**, 066308 (2010).
14. H. B. Squire, "On the stability of three-dimensional disturbances of viscous flow between parallel walls," Proc. R. Soc. London, Ser. A **142**, 129–155 (1933).
15. S. C. Generalis and K. Fujimura, "Range of validity of weakly nonlinear theory in the Rayleigh-Bénard Problem," J. Phys. Soc. Jpn. **78**, 084401 (2009).
16. J. Mizushima and Y. Saito, "Equilibrium characteristics of the secondary convection in a vertical fluid layer between two flat plates," Fluid Dyn. Res. **2**, 183–191 (1987).
17. K. Fujimura and J. Mizushima, in *Nonlinear Wave Interactions in Fluids, Proceedings of the Symposium, Boston, MA, Dec. 13–18, 1987,* Ed. by R. W. Miksad, T. R. Akylas, and T. Herbert (Am. Soc. Mech. Eng., New York, 1987), pp. 123–130.
18. F. H. Busse and R. M. Clever, "Transition to time dependent convection," J. Fluid Mech. **65**, 625–645 (1974).
19. T. Herbert, "Nonlinear stability of parallel flows by high order amplitude expansions," AIAA J. **18**, 1125R (1980).
20. E. C. Aifantis, "Internal Length Gradient (ILG) material mechanics across scales and disciplines," Adv. Appl. Mech. **49**, 1–110 (2016).
21. E. C. Aifantis, "Gradient extension of classical material models: From nuclear to condensed matter scales to earth and cosmological states," in *Size-Dependent Continuum Mechanics Approaches,* Ed. by E. Ghavanloo et al., Vol. 2 of *Springer Tracts in Mechanical Engineering* (Springer Nature, Switzerland, AG, 2021), pp. 417–452.
22. A. Raees, H. Xu, and E. C. Aifantis, "Homotopy shear bound solutions in gradient plasticity," Zeitschr. Naturforsch. **A72**, 477–486 (2017).